PHYSICAL REVIEW B **78**, 184402 (2008)

Field-induced staggered magnetic moment in the quasi-two-dimensional organic Mott insulator κ-(BEDT-TTF)$_2$Cu[N(CN)$_2$]Cl

F. Kagawa,* Y. Kurosaki, K. Miyagawa, and K. Kanoda
Department of Applied Physics, University of Tokyo, Bunkyo-ku, Tokyo 113-8656, Japan
(Received 22 August 2008; published 5 November 2008)

We investigated the magnetism under a magnetic field in the quasi-two-dimensional organic Mott insulator κ-(BEDT-TTF)$_2$Cu[N(CN)$_2$]Cl through magnetization and ^{13}C-NMR measurements. We found that in the nominally paramagnetic phase (i.e., above Néel temperature) the field-induced local moments have a staggered component perpendicular to the applied field. As a result, the antiferromagnetic transition well defined at a zero field becomes crossover under a finite field. This unconventional behavior is qualitatively reproduced by the molecular-field calculation for Hamiltonian including the exchange, Dzyaloshinsky-Moriya (DM), and Zeeman interactions. This calculation also explains other unconventional magnetic features in κ-(BEDT-TTF)$_2$Cu[N(CN)$_2$]Cl reported in the literature. The present results highlight the importance of the DM interaction in field-induced magnetism in a nominally paramagnetic phase, especially in low-dimensional spin systems.

DOI: 10.1103/PhysRevB.78.184402 PACS number(s): 75.30.Kz, 74.70.Kn, 74.25.Nf, 68.35.Rh

I. INTRODUCTION

The quasi-two-dimensional (quasi-2D) organic conductor, κ-(BEDT-TTF)$_2$X, exhibits various phases, depending on anion X, temperature and pressure, and have provided a good experimental stage for investigating fundamental problems in condensed-matter physics[1] [BEDT-TTF, abbreviated as ET hereafter, is bis(ethylenedithio)tetrathiafulvalene]. For instance, κ-(ET)$_2$Cu[N(CN)$_2$]Br and κ-(ET)$_2$Cu(NCS)$_2$ show unconventional superconductivity at ambient pressure,[2,3] and intensive studies regarding its origin are in progress.[4] κ-(ET)$_2$Cu[N(CN)$_2$]Cl (hereafter abbreviated as κ-Cl) is a Mott insulator and suitable for the study of the bandwidth-controlled Mott transition because this material undergoes the Mott transition by soft pressure ($\sim$25 MPa).[5] In fact, recent experiments on κ-Cl using the pressure-sweep technique have revealed fundamental aspects of the Mott transition: the first-order transition with a finite-temperature critical end point ($T_{cr}\sim 40$ K) (Refs. 6–10) and unconventional critical exponents of the Mott criticality.[11] Another interesting aspect in κ-(ET)$_2$X is the magnetism on the frustrated triangular lattice. As will be seen in Sec. II, κ-(ET)$_2$X has an anisotropic triangular lattice where localized moments with antiferromagnetic (AF) correlation are subject to the so-called spin frustration. In this context, the Mott insulator κ-(ET)$_2$Cu$_2$(CN)$_3$ is an intriguing material because it has nearly isotropic triangular lattice. In fact, neither the Néel order nor spin-gapped behavior is observed down to 32 mK in NMR (Refs. 12 and 13) and μSR measurements.[14] A quantum spin liquid has been suggested as the possible ground state of κ-(ET)$_2$Cu$_2$(CN)$_3$.[15,16]

In this paper, we focus on the magnetism of the Mott insulator, κ-Cl. Now, its magnetism is understood as follows: the AF transition occurs at $T_N\sim 27$ K accompanied by weak ferromagnetism, which is due to the canting of antiferromagnetically ordered spins.[17] This canting is attributed to the Dzyaloshinsky-Moriya (DM) interaction, which is inherent in the κ-(ET)$_2$X (see Sec. II). However, further investigations seem to be needed. For instance, Hamad *et al.*[18] found two curious features in ^{1}H-NMR measurements; with increasing magnetic field from 0.58 to 9.3 T, the peak structure of spin-lattice relaxation rate $1/T_1$ around T_N is strongly suppressed and the peak temperature (usually regarded as T_N) increases from $\sim$22 to $\sim$28 K although in conventional antiferromagnets $1/T_1$ is field insensitive and T_N is robust (or decreases under strong field). Hamad *et al.*[18] interpreted the field-dependent $1/T_1$ as a consequence of slow spin dynamics due to the spin frustration; however, the unexpected increase in the nominal T_N with magnetic field remains puzzling.

To get more insight into the magnetism of κ-Cl, we combined magnetization and NMR measurements. On the basis of the experimental results, we argue that the AF transition at a zero magnetic field changes into crossover under a finite field. This statement leads to an intuitively strange consequence that field-induced local spin moments in the paramagnetic phase have a staggered component as well as the uniform one, but we actually found the noncollinear state under a magnetic field. We also performed the molecular-field analysis of Heisenberg model including the DM and Zeeman interactions and succeeded in reproducing qualitatively not only our findings but also the two curious features found by Hamad *et al.*[18] This means that the above-mentioned puzzling magnetism under magnetic field is the manifestation of the interplay between DM and Zeeman interactions. To our knowledge, the importance of DM interaction in a nominally paramagnetic phase has not been recognized so far. In this paper, we demonstrate that the DM interaction plays a key role in the magnetism under magnetic field even above T_N, especially in low-dimensional spin systems.

II. CRYSTAL STRUCTURE OF κ-(ET)$_2$X

κ-(ET)$_2$X has a quasi-2D layered structure composed of conducting ET layers and insulating anion layers [Fig. 1(a)]. In the conducting layer, ET molecules form dimers with

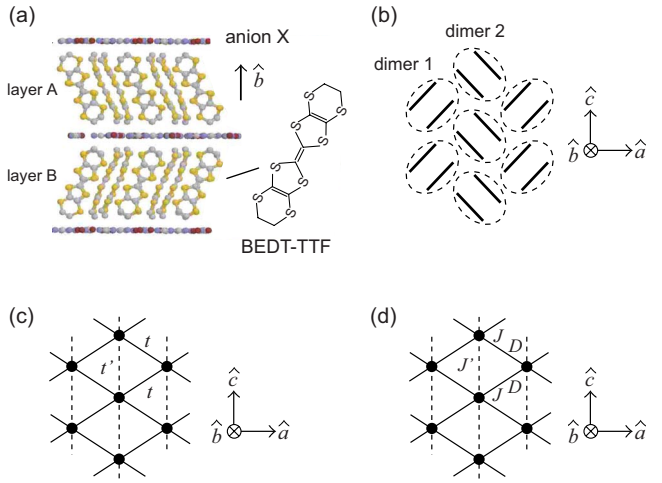

FIG. 1. (Color online) (a) Side view of crystal structure of κ-Cl. (b) Top view of schematic crystal structure of the conducting ET layer. The pair of lines represents a $(ET)_2$ dimer. (c) Dimer-lattice model of the conducting layer in κ-Cl. (d) Localized spin model applicable to κ-Cl.

face-to-face configuration [Fig. 1(b)]. The monovalent anion X introduces a hole into an antibonding dimer orbital, which forms a two-dimensional half-filled band through the interdimer transfer integrals. Thus the dimer lattice can be reduced to an isosceles triangular lattice as shown in Fig. 1(c), which is characterized by two interdimer transfer integrals, t and t'. In the case of the Mott insulating κ-$(ET)_2X$, such as κ-Cl (space-group *Pnma*), a hole is localized at a dimer. Because of the triangular lattice, the localized spins with AF correlation are subject to the spin frustration, of which strength is characterized by the ratio t'/t. The t'/t of κ-Cl is estimated at $\sim$0.75 (i.e., anisotropic triangular lattice).[12] The unit cell of κ-Cl extends over two adjacent conducting layers [layer A and layer B, see Fig. 1(a)] and the each layer includes two inequivalent dimers [dimer 1 and dimer 2, see Fig. 1(b)]. Thus, the unit cell turns out to contain four inequivalent dimers: A1 and A2 in layer A, and B1 and B2 in layer B. These notations are after Ref. 19.

When the magnetism of κ-Cl is discussed in terms of the localized spin model, t and t' are replaced by AF exchange interactions, J and J', respectively. However, one should keep in mind that the DM interaction also works between the nearest dimers [Fig. 1(d)] because the local inversion symmetry is absent between dimer 1 and dimer 2 [see Fig. 1(b)]. In fact, as seen below, the puzzling magnetism found under a magnetic field is understood as a consequence of the DM interaction.

III. EXPERIMENTAL

A. Magnetization measurements

To know the macroscopic magnetism of κ-Cl, we performed magnetization measurements at 0 and 7 T with a superconducting quantum interference device (SQUID) magnetometer. In the measurement of spontaneous weak ferromagnetism under 0 T, κ-Cl was first cooled down to 2 K under 0.1 T (parallel to the conducting layer) and then the magnetic field was switched off. Finally, the magnetization along the plane was measured in an ascending temperature process under 0 T. The uniform spin susceptibility $\chi_{\rm spin}$ at 7 T was obtained after subtracting the core diamagnetism [-4.7×10^{-4} emu/(mol f.u.)] from the measured susceptibility, which was determined by the magnetization divided by the applied magnetic field.

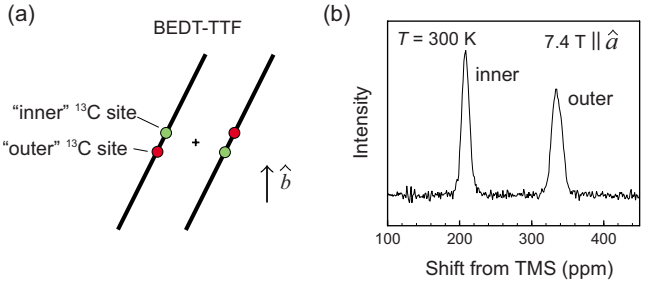

FIG. 2. (Color online) (a) Side view of ET dimer. The cross mark represents the center of the dimer. (b) ^{13}C-NMR spectrum of κ-Cl under $\boldsymbol{H}\|\hat{a}$ at room temperature.

B. NMR measurements

In the NMR measurements, we used a κ-Cl crystal where two central carbon sites in ET molecule are substituted by ^{13}C isotope (hereafter abbreviated as κ-$^{13}C_2$-Cl). Under the field applied in an arbitrary direction, κ-$^{13}C_2$-Cl shows 16 ^{13}C resonance lines at most. This line profile arises from the following three factors.[20] First, as described above, there are four inequivalent dimers in the unit cell: A1, A2, B1, and B2. Second, the inclined face-to-face geometry of ET molecules in the dimer makes the two central ^{13}C sites in ET inequivalent [Fig. 2(a)]: the ^{13}C site closer to the center of the dimer is labeled with "inner" and the other ^{13}C is labeled with "outer." Finally, a nuclear dipolar splitting between the central ^{13}C sites doubles the number of lines. Below we deal mainly with the outer site since the NMR properties of the inner and outer sites show the similar behavior.

In the present NMR measurements, the magnetic field $\boldsymbol{H}$ of 7.4 T was applied parallel to the $\hat{a}$ axis. In that case, the NMR shift of the outer site at dimer i (=A1,A2,B1,B2), K_i^a (in ppm), is given by

$$K_i^a = A_i^{aa}\frac{M_i^a}{H} + A_i^{ab}\frac{M_i^b}{H} + A_i^{ac}\frac{M_i^c}{H} + C_i^a, \qquad (1)$$

where M_i^α denotes the α-axis (α=a,b,c) component of the local spin moment $\boldsymbol{M}_i$ at dimer i, $A_i^{\alpha\alpha}$ is a component of the hyperfine coupling tensor of the outer site in dimer i, and C_i^a (in ppm) is the chemical shift of the site. As discussed by Smith *et al.*,[19] $A_{A1}^{\alpha\alpha}$ is positive for every α and the hyperfine coupling constants at other dimers can be determined by applying the symmetry operation inherent in κ-Cl to $A_{A1}^{\alpha\alpha}$ (space-group *Pnma*). The derived relations between the hyperfine coupling constants at different dimers are as follows:

$$A_{A1}^{aa} = A_{A2}^{aa} = A_{B1}^{aa} = A_{B2}^{aa} > 0, \qquad (2)$$

$$A^{ab}_{A1} = A^{ab}_{A2} = -A^{ab}_{B1} = -A^{ab}_{B2} > 0, \quad (3)$$

$$A^{ac}_{A1} = -A^{ac}_{A2} = A^{ac}_{B1} = -A^{ac}_{B2} > 0. \quad (4)$$

Under $\boldsymbol{H} \| \hat{a}$, the dipolar splitting nearly vanishes because $\boldsymbol{H}$ approximately forms the so-called magic angle (~54.7°) against the ^{13}C=^{13}C vector in ET by happenstance. At room temperature (in the paramagnetic state), all dimers are equivalent under $\boldsymbol{H} \| \hat{a}$; thus ^{13}C-NMR spectra of κ-$^{13}C_2$-Cl shows only two lines coming from the inner ^{13}C and outer ^{13}C [Fig. 2(b)]. A marked feature in the experimental results is that the two-line shape holds even at low temperatures where the spins are ordered. This means that $K^a_{A1}=K^a_{A2}=K^a_{B1}=K^a_{B2}$ is satisfied in the whole temperature range. By using Eqs. (1)–(4), this relation is rewritten as follows:

$$M^a_{A1} = M^a_{A2} = M^a_{B1} = M^a_{B2}, \quad (5)$$

$$M^b_{A1} = M^b_{A2} = -M^b_{B1} = -M^b_{B2}, \quad (6)$$

$$M^c_{A1} = -M^c_{A2} = M^c_{B1} = -M^c_{B2}. \quad (7)$$

Equations (5)–(7) put strict constraints on the spin configuration under $\boldsymbol{H} \| \hat{a}$. In Sec. IV, we determine the spin structure at low temperatures on the basis of these constraints. The absolute values of the Knight shift in the present study are calibrated with the room-temperature line position of the outer site, which is determined to be 336.2 ppm by Smith *et al.*[19]

IV. EXPERIMENTAL RESULTS

In this section, by investigating the macroscopic and microscopic magnetisms of κ-Cl, we demonstrate (i) the increasing "T_N" with a magnetic field and (ii) the field-induced noncollinear local moment in a paramagnetic phase. First we show the macroscopic magnetism. The temperature dependence of χ_{spin} of a κ-Cl single crystal measured at 7 T (parallel to the conducting layer) is presented in the inset of Fig. 3. The result is consistent with χ_{spin} of the powdered sample measured at 0.1 T.[21] The weak ferromagnetism observed below 30 K is due to the DM interaction and therefore should appear spontaneously even under a zero field. In fact, as shown in the main panel of Fig. 3, the magnetization measurements at a zero field confirm a spontaneous weak ferromagnetism parallel to the conducting plane below ~23 K. This temperature is regarded as T_N at a zero field (abbreviated as the zero-field T_N hereafter) and is in good agreement with the peak temperature of $1/T_1$ under 0.58 T.[18] Note that the zero-field T_N is appreciably lower than the peak temperature under 3.7 T (~27 K).[17] Thus, the present results support the finding by Hamad *et al.*[18] that T_N seems to increase with magnetic field (actually, as seen below, the peak temperature of $1/T_1$ should be regarded as crossover temperature rather than ordering temperature in κ-Cl).

Next, we turn to the microscopic magnetism of κ-Cl. Figure 4(a) shows the temperature dependence of ^{13}C-NMR shift at the outer site. The large shift toward low temperatures reflects the growth of local moment, consistent with the

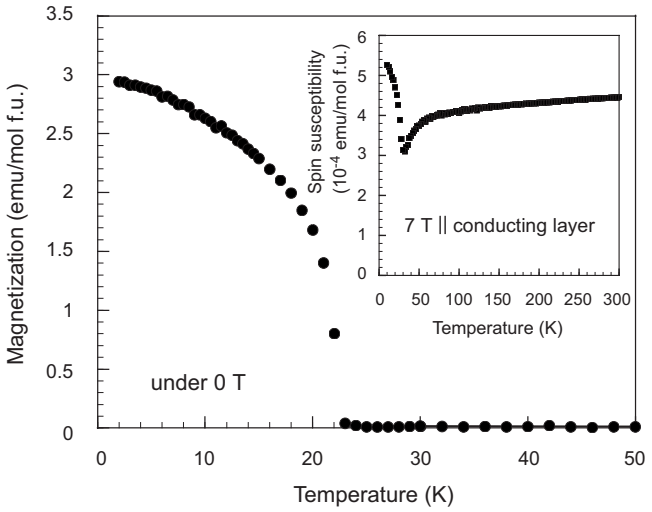

FIG. 3. Temperature dependence of magnetization under a zero magnetic field. Inset: Temperature dependence of spin susceptibility measured under 7 T (parallel to the conducting layer).

previous report.[19] As demonstrated by Smith *et al.*,[19] the spin configuration at low temperatures can be determined by considering this shift in the light of Eqs. (1)–(7). We describe this procedure in more detail, which leads us to conclude the field-induced noncollinear state, one of the findings in the present study. Since the applied field of 7.4 T ($\|\hat{a}$) is far greater than the spin-flop field,[17] the local moments lie nearly in the bc plane with a slight canting toward the field direction ($\|\hat{a}$); moreover, the AF interaction between A1 and A2 makes the b and c components of local moments antiparallel;

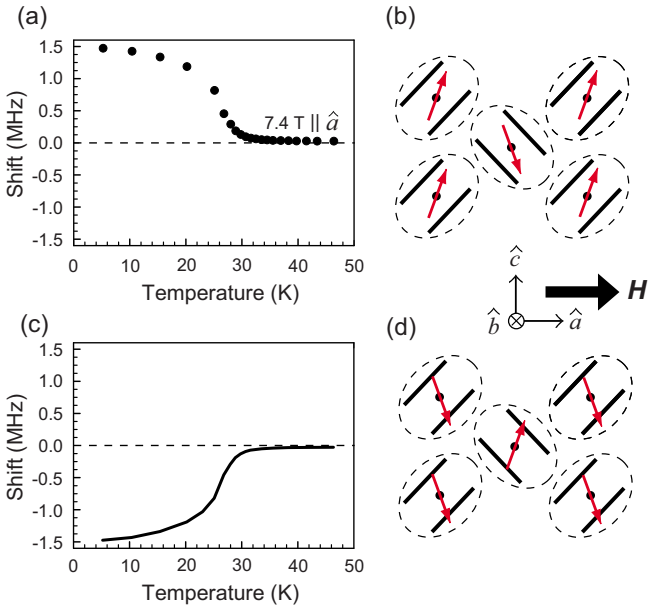

FIG. 4. (Color online) (a) Experimental ^{13}C-NMR shift of the outer site under 7.4 T parallel to the $\hat{a}$ axis. (b) Spin structure at low temperatures deduced from (a). (c) Hypothetical ^{13}C-NMR shift of the outer site and (d) spin structure at low temperatures deduced from (c). The horizontal lines in (a) and (c) represent the shift origin. In (b) and (d), the canting of local moments toward the $\hat{a}$ axis is exaggerated.

thus $M^b_{A1}=-M^b_{A2}$ and $M^c_{A1}=-M^c_{A2}$. From these constraints and Eq. (6), it turns out that the local moments cannot have the b component, i.e., $M^b_{A1}=M^b_{A2}=0$. Thus K^a_{A1} [see Eq. (1)] is given by

$$K^a_{A1}=A^{aa}_{A1}\frac{M^a_{A1}}{H}+A^{ac}_{A1}\frac{M^c_{A1}}{H}+C^a_{A1}. \tag{8}$$

While the sign of magnetization component parallel to the field, M^a_{A1}, is obviously positive, that of the perpendicular component, M^c_{A1}, is not trivial. However, it can be judged explicitly from the sign of the shift at low temperatures where $|M^c_{A1}|\gg M^a_{A1}>0$ and therefore the second term is dominant in Eq. (8). Because $A^{ac}_{A1}>0$ as mentioned above (Sec. III B), the large positive shift below T_N is attributed to the growth of positive M^c_{A1}. In this way, all components of the local moment at dimer A1 at low temperatures are determined to be $M^c_{A1}\gg M^a_{A1}>0$ and $M^b_{A1}=0$. By applying Eqs. (5)–(7) to $\boldsymbol{M}_{A1}$, one finally obtains the whole spin configuration at low temperatures, which is roughly sketched in Fig. 4(b).

Figure 4(a) represents an anomalous feature overlooked in the previous studies: on cooling, the NMR spectra always show the positive shift, i.e., the negative shift as shown in Fig. 4(c) has never been observed. This indicates that at low temperatures the spin configuration having the negative M^c_{A1} as shown in Fig. 4(d) never appears. Note that such situation is not expected in the conventional AF transition under a magnetic field where the Figs. 4(b) and 4(d) configurations are degenerate and thus have the equal chance to emerge below T_N. Therefore, the present result implies that the former configuration has a lower energy than the latter. As seen in Sec. V, the origin of this energy difference is actually understood by considering the DM interaction with the antisymmetric nature, i.e., $\boldsymbol{D}_{12}\cdot(\boldsymbol{S}_1\times\boldsymbol{S}_2)\neq\boldsymbol{D}_{12}\cdot(\boldsymbol{S}_2\times\boldsymbol{S}_1)$. The point is that the thermal average of the two configurations yields positive M^c_{A1} (staggered component) as well as positive M^a_{A1} *regardless of temperature* because of the energy difference, whatever the origin is. In this way, the inevitable positive shift in Fig. 4(a) turns out to indicate that the field-induced local moments under $\boldsymbol{H}\|\hat{a}$ are not uniform ($M^a_i>0$ and $M^c_i=0$) but noncollinear ($M^a_i>0$ and $M^c_{A1}=-M^c_{A2}>0$) even above zero-field T_N.

The noncollinear spin state can be identified more evidently when the uniform $\chi_{\rm spin}$ is compared with the NMR shift K^a_{A1}. Figure 5 shows the temperature dependence of NMR shift ($\boldsymbol{H}\|\hat{a}$) and in-plane $\chi_{\rm spin}$. We assume that the in-plane anisotropy of $\chi_{\rm spin}$ is negligibly small, as is the case in most of the organic conductors. Therefore, the uniform $\chi_{\rm spin}$ can be interpreted as probing M^a_{A1}. Note that when the field-induced local moments under $\boldsymbol{H}\|\hat{a}$ are uniform ($M^a_i>0$ and $M^c_i=0$) as usual, $\chi_{\rm spin}$ and K^a_{A1} should show the same temperature dependence because K^a_{A1} is given by $A^{aa}_{A1}M^a_{A1}/H+C^a_{A1}$ in this case [see Eq. (8)]. As seen in Fig. 5, however, the two quantities exhibit quite different temperature dependence above the zero-field T_N. Especially, the difference is pronounced in 30–60 K: the shift increases on cooling, indicating the growth of local magnetization, while the uniform $\chi_{\rm spin}$ (i.e., M^a_{A1}) decreases. This remarkable disagreement demonstrates that the finite staggered moment $M^c_{A1}(=-M^c_{A2}>0)$ contributes to the observed shift in 30–60 K.

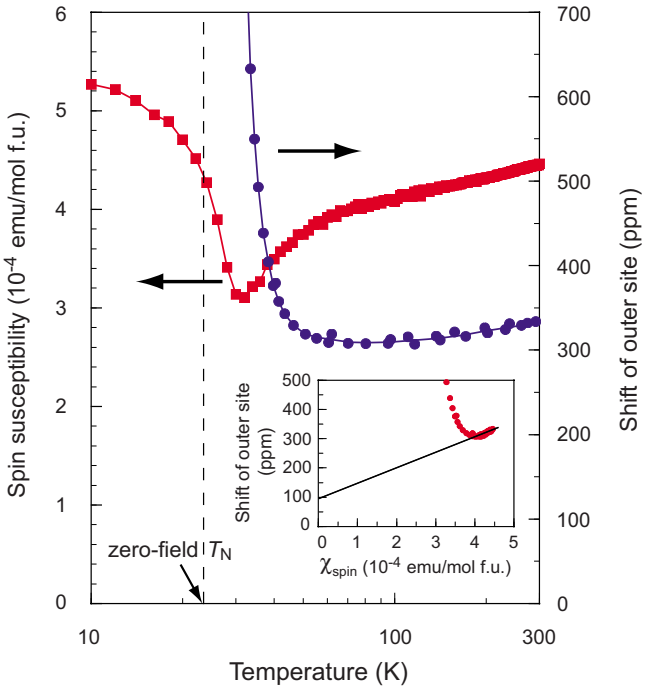

FIG. 5. (Color online) Spin susceptibility measured under 7 T and ^{13}C-NMR shift of the outer site. Solid lines are guide for the eyes. Inset: K-χ plot. The hyperfine coupling constant was estimated from the linear fitting shown in the inset.

Using the reported data of $A^{ac}_{A1}=1.26A^{aa}_{A1}$ and $C^a_{A1}=96$ (ppm),[19,20] we can estimate the magnitude of staggered moment semiquantitatively as follows. Here, K^a_{A1} (ppm) is given by $A^{aa}_{A1}(M^a_{A1}/H+1.26M^c_{A1}/H)+96$. At high temperatures, it is plausible that the field-induced local moment is nearly parallel to the magnetic field (i.e., $M^a_{A1}\gg M^c_{A1}$). Therefore K^a_{A1} around room temperature is given by $A^{aa}_{A1}M^a_{A1}/H+96$, and A^{aa}_{A1} can be estimated roughly from the K-χ plot of the high-temperature data, as shown in the inset of Fig. 5. Note again that the difference between the observed shift and $A^{aa}_{A1}M^a_{A1}/H+96$ (i.e., the straight line in the inset) is attributed to the contribution of staggered component, $A^{ac}_{A1}M^c_{A1}(=1.26A^{aa}_{A1}M^c_{A1})$; thus, using the obtained A^{aa}_{A1}, one can evaluate the temperature dependence of the staggered component M^c_{A1} as well as that of the uniform component M^a_{A1}. The results are shown in Fig. 6(a), where the staggered component $M^c_{A1}(=-M^c_{A2})$ starts to grow markedly below ~60 K. The temperature dependence of noncollinear angle θ defined by $\arctan(M^c_{A1}/M^a_{A1})$ is shown in Fig. 6(b), which demonstrates that with lowering temperature the field-induced noncollinear local moments gradually tilt in accordance with the growth of staggered component.

Note again that the positive staggered moment is induced by a magnetic field even above T_N. Therefore the AF symmetry breaking occurs in the whole temperature range under a field although its degree is expected to vanish asymptotically toward high temperatures. Thus, the rapid increase in the staggered moment, which has so far been addressed

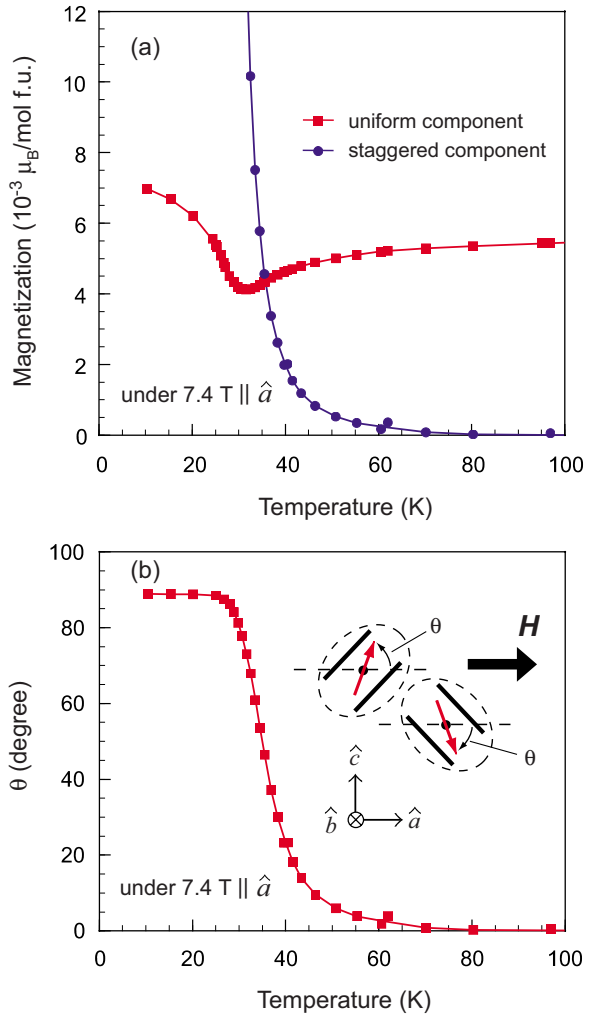

FIG. 6. (Color online) Estimated temperature dependence of (a) the uniform and staggered moment under 7.4 T and (b) the noncollinear angle θ measured from the magnetic-field axis. Eye guides are shown together.

nominally as the AF transition, is not a phase transition but a crossover without thermodynamic singularity. As seen in Sec. V, the crossover behavior under a magnetic field is also demonstrated in the molecular-field calculations.

V. NUMERICAL RESULTS: MOLECULAR-FIELD APPROXIMATION

A. Model Hamiltonian

To reveal the origin of the unconventional magnetism highlighted above, we investigate the $S=1/2$ AF Heisenberg model including the DM and Zeeman interactions on a two-dimensional square lattice [Fig. 7(a)]. Here,

$$\mathcal{H} = J\sum_{\langle i,j\rangle} \boldsymbol{S}_i \cdot \boldsymbol{S}_j + g\mu_B \sum_i \boldsymbol{S}_i \cdot \boldsymbol{H}_i + \sum_{\langle i,j\rangle} \boldsymbol{D}_{ij} \cdot (\boldsymbol{S}_i \times \boldsymbol{S}_j), \quad (9)$$

where $\boldsymbol{S}_i$ and $\boldsymbol{H}_i$ are the spin operator and external magnetic field, respectively, at site i and $\langle \ldots \rangle$ denotes the sum over the nearest neighbors. For simplicity, the DM vector $\boldsymbol{D}$ is set to

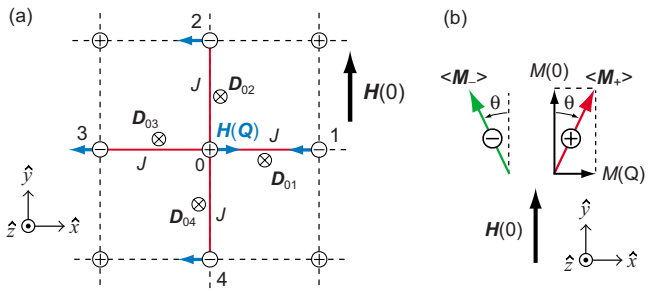

FIG. 7. (Color online) (a) Schematic illustration of the present square-lattice model in the presence of uniform and staggered fields. The local moment at site 0 interacts with four nearest-neighbor sites, 1–4. + and − denote the two magnetic sublattices (see the text). (b) Definition of the uniform moment $M(0)$, staggered moment $M(\boldsymbol{Q})$, and noncollinear angle θ.

be parallel to the $\hat{z}$ axis, and we ignore the AF exchange between the next-nearest neighbors. A uniform field $\boldsymbol{H}(\boldsymbol{q}=0)$ is applied along the $\hat{y}$ axis, where $\boldsymbol{q}$ is a wave-number vector. In the case that only the AF exchange term is present (i.e., $\boldsymbol{H}_i=\boldsymbol{D}_{ij}=0$), the Néel order with $\boldsymbol{Q}=(\pi,\pi)$ is emergent at low temperatures; thus the square lattice can be divided into two magnetic sublattices, + and −, as shown in Fig. 7(a). We choose the $\hat{x}$ axis as the easy axis, but the magnetic anisotropy is not taken into account explicitly.

In this section, we solve the present model using the molecular-field approximation on the two magnetic sublattices. The molecular-field Hamiltonian of Eq. (9) is given by

$$\mathcal{H} = g\mu_B \sum_{i+} \boldsymbol{S}_{i+} \cdot \boldsymbol{H}_+^{\text{eff}} + g\mu_B \sum_{i-} \boldsymbol{S}_{i-} \cdot \boldsymbol{H}_-^{\text{eff}}. \quad (10)$$

Here $i+$ ($i-$) denotes a lattice point on the + (−) magnetic sublattice and $\boldsymbol{H}_+^{\text{eff}}$ ($\boldsymbol{H}_-^{\text{eff}}$) is the effective field perceived by the + (−) magnetic sublattice. The effective field is described by the sum of the external and molecular fields;

$$\boldsymbol{H}_+^{\text{eff}} = -\frac{ZJ}{(g\mu_B)^2}\langle \boldsymbol{M}_- \rangle - \frac{Z}{(g\mu_B)^2}\langle \boldsymbol{M}_- \rangle \times \boldsymbol{D}_{+-} + \boldsymbol{H}_i, \quad (11)$$

$$\boldsymbol{H}_-^{\text{eff}} = -\frac{ZJ}{(g\mu_B)^2}\langle \boldsymbol{M}_+ \rangle - \frac{Z}{(g\mu_B)^2}\boldsymbol{D}_{+-} \times \langle \boldsymbol{M}_+ \rangle + \boldsymbol{H}_i. \quad (12)$$

Here $\boldsymbol{D}_{+-}$ is along the $\hat{z}$ axis, $Z=4$ is the number of the nearest neighbors, and $\langle \boldsymbol{M}_+ \rangle$($\langle \boldsymbol{M}_- \rangle$) denotes the statistically averaged local moments on the +(−) sublattices. In the molecular-field solutions, $\langle \boldsymbol{M}_+ \rangle$ and $\langle \boldsymbol{M}_- \rangle$ are determined self-consistently so as to satisfy $\langle \boldsymbol{M}_+ \rangle \| \boldsymbol{H}_+^{\text{eff}}$ and $\langle \boldsymbol{M}_- \rangle \| \boldsymbol{H}_-^{\text{eff}}$. Note that because of Zeeman and DM terms such local moments are symmetric with respect to the $\hat{y}$ axis [$\|\boldsymbol{H}(0)$] and lie in the $\hat{x}$-$\hat{y}$ plane. For clarity, we adopt the basis composed of the uniform moment along the $\hat{y}$ axis, $M(0)=|\langle \boldsymbol{M}_+ \rangle + \langle \boldsymbol{M}_- \rangle|/2$, and the staggered moment along the $\hat{x}$ axis, $M(\boldsymbol{Q})=|\langle \boldsymbol{M}_+ \rangle - \langle \boldsymbol{M}_- \rangle|/2$, as illustrated in Fig. 7(b). We define the noncollinear angle θ as $\arctan^{-1}[M(\boldsymbol{Q})/M(0)]$. When we calculate the staggered susceptibility $\chi(\boldsymbol{Q})$ under $\boldsymbol{H}(0)$, a staggered field $\boldsymbol{H}(\boldsymbol{Q})$ is applied additionally along the $\hat{x}$ axis [see Fig. 7(a)]; then $\chi(\boldsymbol{Q})$ is obtained from the difference of

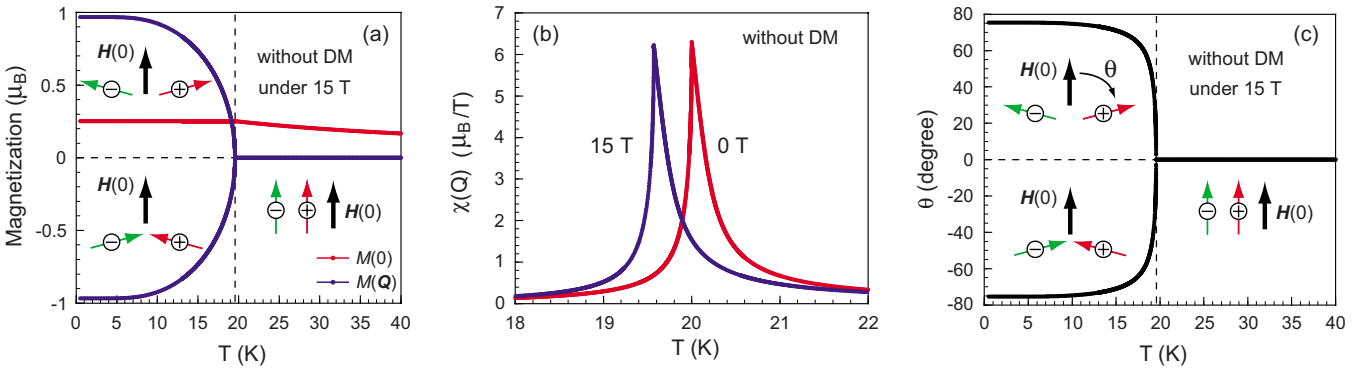

FIG. 8. (Color online) Molecular-field calculation of temperature dependence of (a) the uniform magnetization $M(0)$ and the staggered magnetization $M(\boldsymbol{Q})$ under 15 T, (b) the staggered susceptibility $\chi(\boldsymbol{Q})$ under 0 and 15 T, and (c) the noncollinear angle θ under 15 T. In the present calculations, the DM interaction is not included.

$M(\boldsymbol{Q})$ between under $\boldsymbol{H}(0)$ and under $\boldsymbol{H}(0)+\boldsymbol{H}(\boldsymbol{Q})$, as represented in the following equation:

$$\chi(\boldsymbol{Q}) \equiv \frac{M[\boldsymbol{Q},\boldsymbol{H}(0)+\boldsymbol{H}(\boldsymbol{Q})]-M[\boldsymbol{Q},\boldsymbol{H}(0)]}{|\boldsymbol{H}(\boldsymbol{Q})|}. \quad (13)$$

Although $\chi(\boldsymbol{Q})$ should be calculated under an infinitesimal $\boldsymbol{H}(\boldsymbol{Q})$, the present calculation of $\chi(\boldsymbol{Q})$ was performed under $|\boldsymbol{H}(\boldsymbol{Q})|=20$ mT because of the finite numerical accuracy. Below, within the molecular-field approximation, we show the temperature dependence of $M(0)$, $M(\boldsymbol{Q})$, and $\chi(\boldsymbol{Q})$ under various magnitudes of $\boldsymbol{H}(0)$ and $\boldsymbol{D}_{+-}$. Throughout the calculation, $J=20$ K and $g=2$ were used. The molecular-field T_N in the square lattice under a zero field is given by $\sqrt{J^2+|\boldsymbol{D}_{+-}|^2}$. Hence in the case of $|\boldsymbol{D}_{+-}|=0$, T_N equals J, namely, 20 K.

B. Heisenberg model without DM interaction under magnetic field

It is instructive to show first the consequences of the Heisenberg model without the DM interaction under a magnetic field. As is well known, the AF transition, which is characterized by the emergence of $M(\boldsymbol{Q})$ and the divergence of $\chi(\boldsymbol{Q})$, is still well defined even under a uniform field of moderate magnitude. This feature is reproduced in our numerical calculation: under 15 T, finite $M(\boldsymbol{Q})$ appears below T_N ($\sim$19.57 K) [Fig. 8(a)] and $\chi(\boldsymbol{Q})$ is divergent at this temperature [Fig. 8(b)] although T_N is suppressed slightly from 20 K.[22] Below T_N, $M(\boldsymbol{Q})$ can either be positive or negative (i.e., parallel or antiparallel to the $\hat{x}$ axis) because the positive- and the negative-$M(\boldsymbol{Q})$ phases are degenerate. The presence of this spontaneous symmetry breaking also assures the well-defined AF transition even under 15 T. Reflecting the well-defined AF transition, the noncollinear state (i.e., finite θ) is emergent only below T_N, as shown in Fig. 8(c).

C. Heisenberg model with DM interaction under magnetic field

Next, we consider the Heisenberg model including the DM interaction under a uniform field $\boldsymbol{H}(0)$ within the molecular-field approximation. The model was found to exhibit the following characteristic features: (i) a uniform field induces the noncollinear local moments even in the paramagnetic phase (i.e., above the zero-field T_N); (ii) the divergence of $\chi(\boldsymbol{Q})$ at T_N is suppressed under a uniform field; and (iii) the peak temperature of $\chi(\boldsymbol{Q})$ increases with the field in a low-field region. Below we explain these properties in sequence.

Under a zero field, the self-consistent moments are zero at high temperatures (i.e., paramagnetic), while the spontaneous local moments appear below the mean-field T_N($=\sqrt{J^2+|\boldsymbol{D}_{+-}|^2}$). In the paramagnetic state, the local moments are induced under a finite field. Note that such field-induced local moments cannot be collinear because the collinear state does not satisfy $\langle \boldsymbol{M}_+\rangle \| \boldsymbol{H}_+^{\mathrm{eff}}$ and $\langle \boldsymbol{M}_-\rangle \| \boldsymbol{H}_-^{\mathrm{eff}}$, as illustrated in Fig. 9(a). Therefore, in a self-consistent result, the field-induced local moments should form a noncollinear configuration characterized by positive $M(0)$ and positive $M(\boldsymbol{Q})$ [Fig. 9(b)] in the whole temperatures. We actually calculated the temperature dependence of the field-induced local moments. Figures 10(a) and 10(b) show the behavior of $M(\boldsymbol{Q})$ and θ, respectively, under $|\boldsymbol{H}(0)|=3$ T with $|\boldsymbol{D}_{+-}|=0.2$, 1, and 3 K. Although $M(\boldsymbol{Q})$ and θ show rapid increase around 20 K on cooling, they are finite in the whole temperature range as expected, demonstrating that the AF transition accompanied by thermodynamic singularity does not occur in the presence of DM and Zeeman interactions. We also note that as $|\boldsymbol{D}_{+-}|$ increases, the noncollinear feature above $\sim$20 K becomes more pronounced over a wide temperature range [Fig. 10(b)].[23]

Figures 11(a) and 11(b) show the temperature dependence of $\chi(\boldsymbol{Q})$ for $|\boldsymbol{D}_{+-}|=0.2$ and 3 K, respectively, under various $\boldsymbol{H}(0)$. As $\boldsymbol{H}(0)$ increases, the $\chi(\boldsymbol{Q})$-divergence emergent at 0 T is gradually suppressed into a rounded peak, consistent with the absence of AF transition. The peak suppression is more prominent for larger $|\boldsymbol{D}_{+-}|$, as seen in Fig. 11(b). These results are in sharp contrast to the magnetic-field effect on $\chi(\boldsymbol{Q})$ without the DM interaction [Fig. 8(b)].

From the experimental point of view, the peak structure of $\chi(\boldsymbol{Q})$ [or $\chi(\boldsymbol{Q})$-related quantities] has often been interpreted as the indication of AF transition. However, we emphasize again that in the presence of DM interaction the peak under a magnetic field should be regarded as the manifestation of the crossover. Therefore we name the peak temperature the

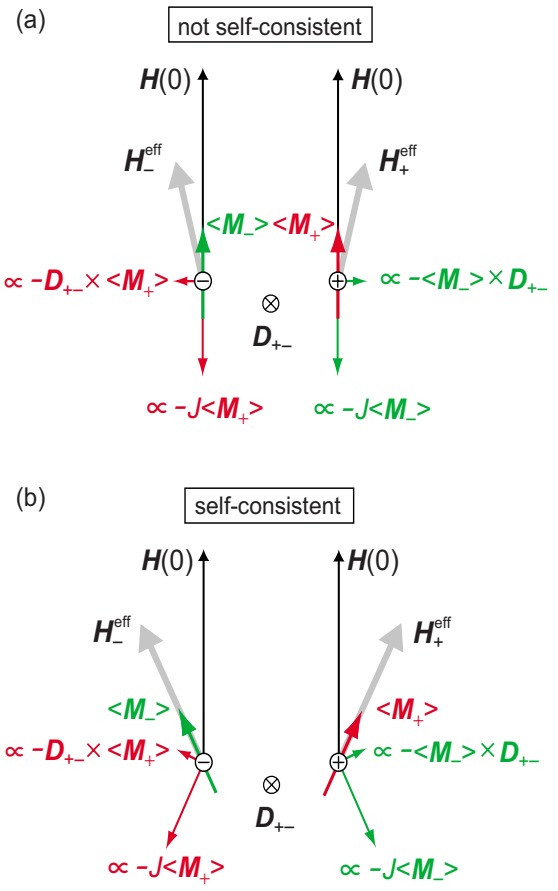

FIG. 9. (Color online) Schematic configuration of the local moments, molecular fields produced by them, and external uniform field for the case of (a) collinear local moments and (b) noncollinear local moments. The effective fields $\boldsymbol{H}_{+}^{\mathrm{eff}}$ ($\boldsymbol{H}_{-}^{\mathrm{eff}}$) perceived by the + (−) sublattices are also shown for each case.

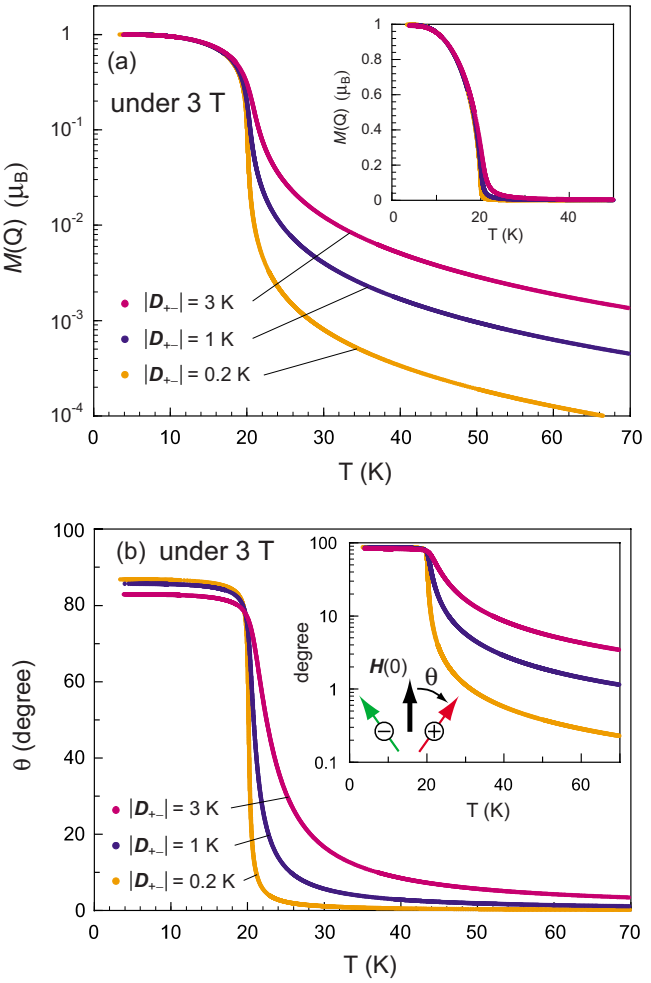

FIG. 10. (Color online) Molecular-field calculations of temperature dependence of (a) the staggered magnetization $M(\boldsymbol{Q})$ and (b) the noncollinear angle θ. Insets: Plots in (a) linear scale and (b) logarithmic scale.

crossover temperature, T^*. The magnetic-field dependence of T_N (at $|\boldsymbol{D}_{+-}|=0$) and T^* (at $|\boldsymbol{D}_{+-}|\neq 0$) is qualitatively different, as shown in Figs. 12(a) and 12(b): T^* increases with $\boldsymbol{H}(0)$ in a low-field region regardless of the strength of $\boldsymbol{D}_{+-}$, while T_N decreases monotonously. The field-dependence of T^* is determined by the superposition of the following two effects. One is the competition between AF exchange and Zeeman interactions, which leads to the suppression of T_N, as is well known. The other is the cooperation between the DM and Zeeman interactions, which is naturally expected from the fact that compared with a collinear-AF state, a canted-AF state is favored by both interactions. This cooperation effect appears in $\triangle T \equiv T^* - T_N$, which is plotted against $|\boldsymbol{H}(0)|$ in Fig. 12(c). In contrast to the case of T_N, $\triangle T$ increases monotonously with $|\boldsymbol{H}(0)|$, and this increase is enhanced for larger $|\boldsymbol{D}_{+-}|$ value. The field dependence of T^* results from the sum of the two effects and thus may show nonmonotonic field dependence such as shown in Fig. 12(a).

VI. DISCUSSION

A. Comparison between the experimental and numerical results

Now we compare the experimental results with molecular-field calculations. The puzzling magnetism found in κ-Cl is summarized as follows: (i) even above the zero-field T_N, the field-induced local moments have a staggered component perpendicular to the applied field, and thus the AF transition is not well defined under a magnetic field; (ii) with increasing magnetic field, the peak structure in the temperature dependence of $1/T_1$ is suppressed;[18] and (iii) the peak temperature in $1/T_1$ increases with the applied field.[18] As seen in Sec. V, the experimental result (i) was reproduced qualitatively by the present calculation. In addition, the calculations showed that the peak structure of $\chi(\boldsymbol{Q})$ is suppressed with increasing $|\boldsymbol{H}(0)|$ (Fig. 11) and that the peak temperature increases in a low-field region [Figs. 12(a) and 12(b)]. Thus, as far as $1/T_1T$ around T_N (or T^*) reflects well $\chi(\boldsymbol{Q})$,[24] the molecular-field results also explain features (ii) and (iii) qualitatively. These agreements between the experimental and molecular-field results indicate that the puzzling magnetism in κ-Cl is essentially due to the interplay between Zeeman and DM interactions. It should be noted that the NMR line shift in the spin system including the DM interaction is not proportional to the macroscopic magnetization even in the nominally paramagnetic state except the high-temperature regime; as was demonstrated by our experimen-

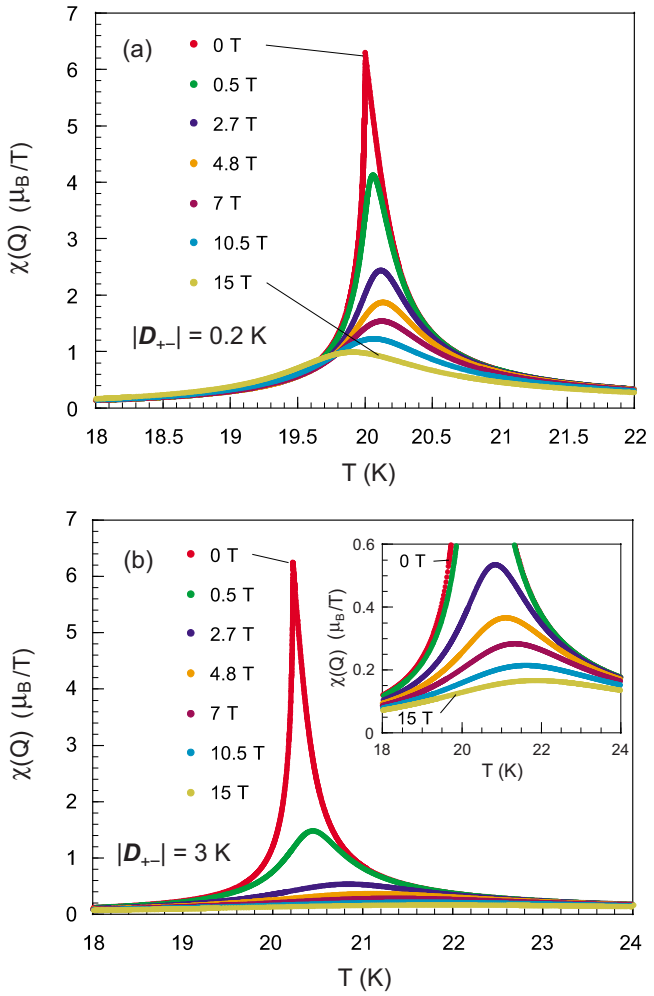

FIG. 11. (Color online) Molecular-field calculations of temperature dependence of $\chi(\boldsymbol{Q})$ under various magnetic-fields at (a) $|\boldsymbol{D}_{+-}|$=0.2 and (b) 3 K. Inset of (b): Enlarged view of low-$\chi(\boldsymbol{Q})$ part.

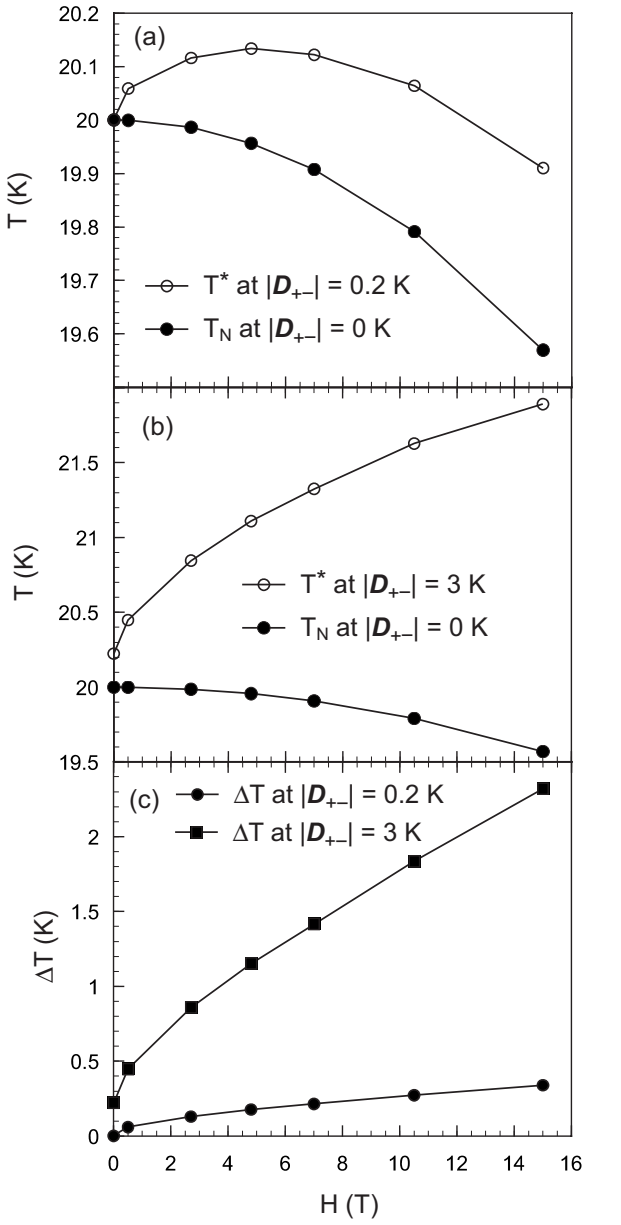

FIG. 12. Molecular-field calculations of magnetic-field dependence of T^* at (a) $|\boldsymbol{D}_{+-}|$=0.2 and (b) 3 K. (c) Molecular-field calculations of magnetic-field dependence of $\triangle T(\equiv T^*-T_N)$ at $|\boldsymbol{D}_{+-}|$ =0.2 and 3 K. For comparison, the magnetic-field dependence of T_N at $|\boldsymbol{D}_{+-}|$=0 K is also shown in (a) and (b).

tal and numerical results, a magnetic field induces the noncollinear spin configuration and thus the NMR line shift reflects not only the uniform component but also the staggered component of local moments.

B. Quantitative disagreement between the experimental and molecular-field results

The agreement between the unconventional magnetism of κ-Cl and the molecular-field results is qualitative but not quantitative; the features revealed by the calculations are highly enhanced in the experimental observations. In κ-Cl, D/J is considered to be 10^{-3}–10^{-2} (Ref. 19); therefore the molecular-field results for $|\boldsymbol{D}_{+-}|$=0.2 K (hence $D/J=10^{-2}$) should be a relevant reference. However, the unconventional features in the numerical results for $|\boldsymbol{D}_{+-}|$=0.2 K are not as pronounced as those observed in κ-Cl. First, the values of θ above T_N in the numerical results [Fig. 10(b)] are too small to be observed experimentally, while the experimental θ values remain observable even well above T_N [Fig. 6(b)]. Second, the increase in T^* with a uniform field is also tiny (0.7% at most) in the calculations [Fig. 12(a)], while an increase by more than 20% was observed in κ-Cl.[18] When these quantitative deviations are considered from the molecular-field point of view, D/J of κ-Cl seems as if it were much larger than 10^{-2}. These quantitative disagreements imply that some sort of effects beyond the molecular-field treatment enhances the unconventional features induced by the interplay between the DM and Zeeman interactions. Although we have no numerical evidence, we speculate that the most possible candidate is the AF short-range order enhanced by low dimensionality, considering that κ-Cl is actually a quasi-2D system. In fact, the values of T_N/J differ significantly for the molecular-field and experimental results: $T_N/J=1$ in the present

molecular-field results, while T_N/J is less than 0.1 in κ-Cl (the zero-field T_N is ~23 K and J is considered to be of the order of room temperature).[19] In low-dimensional AF spin systems, the AF short-range order and thus $\chi(\boldsymbol{q}_{\mathrm{AF}})$ generally grow toward T_N. This growth may enhance the effective magnitude of the DM interaction, resulting in a more prominent staggered moment and in more field-dependent T^* than expected in the molecular-field calculation.

The molecular-field results do not reproduce the monotonic decrease in χ_{spin} down to ~30 K in κ-Cl [the inset of Fig. 3] even in a qualitative level. This discrepancy is possibly due to the low dimensionality of κ-Cl, and the further investigation of Eq. (9) is needed beyond the molecular-field approximation. On the other hand, it is likely that the magnetism of κ-Cl cannot be described adequately by the model Hamiltonian of Eq. (9) because κ-Cl is located near the Mott transition;[5–11] thus the charge fluctuations are probably not negligible above the critical end point at ~40 K. Therefore the localized spin model may not be adequate to describe the magnetism of κ-Cl at high temperatures. The Hubbard model, which incorporates the charge degrees of freedom, or the Heisenberg model including higher-order exchange interactions are considered more realistic.

C. Comparison with the previous studies

Our explanation of the field-dependent $1/T_1$ in κ-Cl is different from the one proposed by Hamad *et al.*[18] In general, $1/T_1T$ is given by

$$\frac{1}{T_1T} \propto \sum_{\boldsymbol{q}} \frac{\mathrm{Im}\,\chi(\boldsymbol{q},\omega_0)}{\omega_0}, \tag{14}$$

where ω_0 is an observing NMR frequency proportional to $|\boldsymbol{H}(0)|$. In most cases, $\mathrm{Im}\,\chi(\boldsymbol{q},\omega)/\omega$ is ω independent at low frequencies of NMR, and hence $1/T_1$ does not depend on a magnetic field. In order to explain the strongly field-dependent $1/T_1$ of κ-Cl, Hamad *et al.*[18] argued that $\mathrm{Im}\,\chi(\boldsymbol{q},\omega)/\omega$ can have ω dependence due to slow spin dynamics under spin frustration. This is a *frequency effect* but not a *field effect* [i.e., the magnetic-field dependence of $\chi(\boldsymbol{q},\omega=0)$ is not considered]. They performed numerical calculations on the Heisenberg model (without the DM interaction) on an anisotropic triangular lattice by using the modified spin-wave theory and reproduced the suppression of $1/T_1$ peak under a uniform field. However their numerical results also exhibit three characteristics inconsistent with the experiments as follows: a double-peak structure appears in the temperature dependence of $1/T_1$; the peak temperature of $1/T_1$ does not depend on $|\boldsymbol{H}(0)|$; and $1/T_1$ depends on a magnetic field over a wider temperature range than observed.

In contrast, we ignore the frequency effect and consider the field dependence of $\chi(\boldsymbol{q},\omega=0)$ in the presence of DM interaction. This is the field effect. Our treatment exhibits the strong field dependence of $\chi(\boldsymbol{Q})$ only around the zero-field T_N [Figs. 11(a) and 11(b)]. As described in Sec. VI A, as far as $\chi(\boldsymbol{q}_{\mathrm{AF}})$ and $1/T_1T$ are well correlated near T_N (or T^*) in κ-Cl,[24] the molecular-field results explain the experimental results without the discrepancies encountered in the model postulated by Hamad *et al.*[18] Thus, the unconventional field dependence of $1/T_1$ observed only around the zero-field T_N is successfully understood in terms of the field effect on $\chi(\boldsymbol{q}_{\mathrm{AF}})$.

The field-induced staggered moment, which is a key consequence of the present study, has often been observed and discussed in quantum disordered or gapped spin systems. Oshikawa and Affleck[25] argued that in $S=1/2$ AF spin chains, the interplay between the Zeeman and DM interactions induces the staggered field perpendicular to the applied magnetic field, resulting in the field-induced staggered moment. This actually explains the observations in Cu benzoate[26] and copper pyrimidine dinitrate.[27] The spin-gapped system with DM interaction, such as NENP ($S=1$ AF spin chain)[28,29] and $SrCu_2(BO_3)_2$ ($S=1/2$ 2D frustrated spin system),[30,31] also show a field-induced staggered moment below a critical field. These properties are also well understood in terms of the staggered-field mechanism. The present study is addressed as the extension of this issue to the quasi-2D spin systems undergoing a finite-temperature AF transition. Recently, the NMR line shift of La_2CuO_4, in which the DM interaction is inherent, has been discussed in terms of the field-induced staggered moment.[32]

VII. CONCLUSION

We performed the magnetization and NMR measurements on κ-(BEDT-TTF)$_2$Cu[N(CN)$_2$]Cl for deeper understanding of its magnetism. We found that the application of a uniform field induces a staggered moment perpendicular to the applied field even above T_N. The molecular-field calculation revealed that the field-induced staggered moment comes from the interplay between the Zeeman and DM interactions and that this interplay explains the several otherwise puzzling magnetic features observed in experiments. By comparing the experiment results with our numerical results, we concluded that the DM interaction affects significantly the field-induced magnetism in a paramagnetic phase especially in low-dimensional systems.

ACKNOWLEDGMENTS

The authors thank M. Takigawa, S. Todo, S. Miyahara, and M. Imada for fruitful discussion and S. Niitaka for his support of SQUID measurements. This work was in part supported by a Grant-in-Aid for Scientific Research in Priority Areas of "Molecular Conductors" (Grant No. 15073204) and "Physics of Superclean Materials" (Grant No. 17071003) from the Ministry of Education, Culture, Sports, Science and Technology, and a Grant-in-Aid for Scientific Research (Grants No. 15104006, No. 20244055, and No. 20540346) from the JSPS.

*Present address: Multiferroics Project (MF), ERATO, Japan Science and Technology Agency (JST), c/o Department of Applied Physics, University of Tokyo, Bunkyo-ku, Tokyo 113-8656, Japan.

[1] K. Kanoda, Physica C **282-287**, 299 (1997); Hyperfine Interact. **104**, 235 (1997); J. Phys. Soc. Jpn. **75**, 051007 (2006).

[2] A. M. Kini, U. Geiser, H. H. Wang, K. D. Carlson, J. M. Williams, W. K. Kwok, K. G. Vandervoort, J. E. Thompson, D. L. Stupka, D. Jung, and M.-H. Whangbo, Inorg. Chem. **29**, 2555 (1990).

[3] H. Urayama, H. Yamochi, G. Saito, K. Nozawa, T. Sugano, M. Kinoshita, S. Sato, K. Oshima, A. Kawamoto, and J. Tanaka, Chem. Lett. **17**(1), 55 (1988).

[4] For review, see B. J. Powell and R. H. McKenzie, J. Phys.: Condens. Matter **18**, R827 (2006).

[5] H. Ito, T. Ishiguro, M. Kubota, and G. Saito, J. Phys. Soc. Jpn. **65**, 2987 (1996).

[6] S. Lefebvre, P. Wzietek, S. Brown, C. Bourbonnais, D. Jérome, C. Mézière, M. Fourmigué, and P. Batail, Phys. Rev. Lett. **85**, 5420 (2000).

[7] D. Fournier, M. Poirier, M. Castonguay, and K. D. Truong, Phys. Rev. Lett. **90**, 127002 (2003).

[8] P. Limelette, P. Wzietek, S. Florens, A. Georges, T. A. Costi, C. Pasquier, D. Jérome, C. Mézière, and P. Batail, Phys. Rev. Lett. **91**, 016401 (2003).

[9] F. Kagawa, T. Itou, K. Miyagawa, and K. Kanoda, Phys. Rev. B **69**, 064511 (2004).

[10] F. Kagawa, T. Itou, K. Miyagawa, and K. Kanoda, Phys. Rev. Lett. **93**, 127001 (2004).

[11] F. Kagawa, K. Miyagawa, and K. Kanoda, Nature (London) **436**, 534 (2005).

[12] Y. Shimizu, K. Miyagawa, K. Kanoda, M. Maesato, and G. Saito, Phys. Rev. Lett. **91**, 107001 (2003).

[13] Y. Shimizu, K. Miyagawa, K. Kanoda, M. Maesato, and G. Saito, Phys. Rev. B **73**, 140407(R) (2006).

[14] S. Ohira, Y. Shimizu, K. Kanoda, and G. Saito, J. Low Temp. Phys. **142**, 153 (2006).

[15] T. Mizusaki and M. Imada, Phys. Rev. B **74**, 014421 (2006).

[16] S.-S. Lee, P. A. Lee, and T. Senthil, Phys. Rev. Lett. **98**, 067006 (2007).

[17] K. Miyagawa, A. Kawamoto, Y. Nakazawa, and K. Kanoda, Phys. Rev. Lett. **75**, 1174 (1995).

[18] I. J. Hamad, A. E. Trumper, P. Wzietek, S. Lefebvre, and L. O. Manuel, J. Phys.: Condens. Matter **17**, 8091 (2005).

[19] D. F. Smith, S. M. De Soto, C. P. Slichter, J. A. Schlueter, A. M. Kini, and R. G. Daugherty, Phys. Rev. B **68**, 024512 (2003).

[20] S. M. De Soto, C. P. Slichter, A. M. Kini, H. H. Wang, U. Geiser, and J. M. Williams, Phys. Rev. B **52**, 10364 (1995).

[21] A. Kawamoto, K. Miyagawa, Y. Nakazawa, and K. Kanoda, Phys. Rev. B **52**, 15522 (1995).

[22] Strictly speaking, our numerical results show not the genuine divergence of $\chi(\boldsymbol{Q})$ but a finite peak value of $\sim 6.28\mu_B/\mathrm{T}$ because $\chi(\boldsymbol{Q})$ was calculated under a finite value of $\boldsymbol{H}(\boldsymbol{Q})$. In our numerical accuracy, the divergence of $\chi(\boldsymbol{Q})$ appears as the peak value larger than $6.2\mu_B/\mathrm{T}$.

[23] Concerning the magnetic-field effect on the noncollinear feature, we also found that θ above the mean-field T_N is almost field independent between under 0.1 and 3 T, while $|\langle \boldsymbol{M}_+ \rangle|$ is nearly proportional to $\boldsymbol{H}(0)$ in this field range (not shown).

[24] Around T_N (or T^*), $1/T_1T$ is generally dominated by $\mathrm{Im}\,\chi(\boldsymbol{q}_{\mathrm{AF}},\omega_0)/\omega_0$, where $\boldsymbol{q}_{\mathrm{AF}}$ and ω_0 represent the wave-number vector of AF order and the observing NMR frequency, respectively. Within the time-dependent Ginzburg-Landau equation, the sign of $\frac{\partial}{\partial T}\chi(\boldsymbol{q}_{\mathrm{AF}},0)$ and $\frac{\partial}{\partial H}\chi(\boldsymbol{q}_{\mathrm{AF}},0)$ agrees with, respectively, that of $\frac{\partial}{\partial T}\mathrm{Im}\,\chi(\boldsymbol{q}_{\mathrm{AF}},\omega_0)/\omega_0$ and $\frac{\partial}{\partial H}\mathrm{Im}\,\chi(\boldsymbol{q}_{\mathrm{AF}},\omega_0)/\omega_0$, as far as ω_0 is lower enough than the characteristic relaxation frequency of the electron-spin dynamics. Thus it is likely that around T_N (or T^*), $\chi(\boldsymbol{q}_{\mathrm{AF}})$ and $1/T_1T$ show the qualitatively similar temperature dependence and magnetic-field dependence.

[25] M. Oshikawa and I. Affleck, Phys. Rev. Lett. **79**, 2883 (1997).

[26] D. C. Dender, P. R. Hammar, D. H. Reich, C. Broholm, and G. Aeppli, Phys. Rev. Lett. **79**, 1750 (1997).

[27] A. U. B. Wolter, P. Wzietek, S. Süllow, F. J. Litterst, A. Honecker, W. Brenig, R. Feyerherm, and H.-H. Klauss, Phys. Rev. Lett. **94**, 057204 (2005).

[28] J. P. Renard, M. Verdaguer, L. P. Regnault, W. A. C. Erkelens, J. Rossat-Mignod, and W. G. Stirling, Europhys. Lett. **3**, 945 (1987).

[29] M. Chiba, Y. Ajiro, H. Kikuchi, T. Kubo, and T. Morimoto, Phys. Rev. B **44**, 2838 (1991).

[30] K. Kodama, M. Takigawa, M. Horvatić, C. Berthier, H. Kageyama, Y. Ueda, S. Miyahara, F. Becca, and F. Mila, Science **298**, 395 (2002).

[31] K. Kodama, S. Miyahara, M. Takigawa, M. Horvatić, C. Berthier, F. Mila, H. Kageyama, and Y. Ueda, J. Phys.: Condens. Matter **17**, L61 (2005).

[32] A. S. Moskvin, Phys. Rev. B **75**, 054505 (2007).